Advanced Soft- and Hard-Magnetic Material Models for the Numerical Simulation of Electrical Machines

Nora Leuning, Silas Elfgen, Benedikt Groschup, Gregor Bavendiek, Simon Steentjes, and Kay Hameyer

Institute of Electrical Machines, RWTH Aachen University, D-50262 Aachen, Germany

Accurate modeling of soft- and hard-magnetic materials for the numerical simulation of rotating electrical machines is required to allow predictions on the operational characteristics along the torque–speed map, already in the design stage. The full potential of most appropriate material selection and concurrent geometry adaption can only be utilized if models can represent actual material behavior. The accurate prediction of iron losses of soft-magnetic materials for various frequencies and magnetic flux densities, as well as the degradation due to manufacturing is eminent for the design of electrical machines. Therefore, advanced material models need to be adapted and their accuracy examined to further improve the modeling and enable progression. This paper will give an overview of the current modeling approaches applied at the Institute of Electrical Machines for soft- and hard-magnetic materials in the simulation of rotating electrical machines. A case example in the form of a traction drive is presented to which the models are applied. For the machine modeling, the inhouse solver pyMOOSE is utilized. In order to determine the losses with regard to manufacturing processes, the iron-loss model with material degradation is used in combination with a machine simulation scheme of the entire operating range of the machine. Here, various simulation approaches are combined to form the entire computational toolchain to obtain accurate results in the entire operational range.

Index Terms— **Electrical machines, hard-magnetic material, numerical simulation, soft-magnetic material.**

I. Introduction

THE development of energy-efficient electrical machines requires an accurate knowledge of the soft- and hard-magnetic material behavior, already in the design stage. Next to the aim of an accurate simulation of the magnetic core of an electric machine including all possible parasitic effects such as tolerances in geometry or material properties, varying operational boundaries, the exact knowledge of the local quantities such as flux density or loss distribution in the core is important to enhance the machine's design. The art of machine design is to determine the best possible core geometry for a particular application by utilizing all knowledge about the used material and its behavior during operation. The soft-magnetic material constitutes the magnetic core of an electrical machine and its properties significantly influence the operating characteristics and efficiency of electrical machines.

On that account, the accurate prediction of iron losses of soft-magnetic materials for various frequencies and magnetic flux densities, i.e., arbitrary magnetic field waveforms, is eminent for the design of electrical machines [1]. This paper is focused on efficient (scalar and local) post-processing calculation of iron losses. Vector hysteresis models are another possibility to determine the iron losses in electrical machines. Due to their strong additional computational effort, they are not the focus of this paper. A comparison of post-processed iron losses versus iron losses calculation during simulation is, however, presented in [2] and an overview of advanced hysteresis models can be found in [3] as well as in [4] with a relation to the materials microstructure.

Manuscript received March 9, 2018; revised June 2, 2018; accepted August 8, 2018. Corresponding author: N. Leuning (e-mail: nora.leuning@iem.rwth-aachen.de).

Color versions of one or more of the figures in this paper are available online at http://ieeexplore.ieee.org.

Digital Object Identifier 10.1109/TMAG.2018.2865096

The objective of this paper is iron-loss models, which describe the loss-generating effects, i.e., hysteresis, non-local eddy currents and excess eddy currents. Most of these suffer from poor accuracy for not considering the effect of high frequencies and high material utilization as well as the material degradation due to the magnetoelastic coupling. This paper presents a comparison of the common iron-loss models to the Institute of Electrical Machines (IEM)-formula. The IEM formula resolves the limitation by introducing a high-order term of the magnetic flux density and can be enhanced to consider the alteration of material-dependent loss-parameters due to the magnetoelastic coupling [5], [6]. IEM's loss formula seems to be more complicated when compared to other approaches using empirical factors to model the material because of its various terms representing particular physical effects. However, the strength of this formula can be seen in the possibility to reliably identify operational conditions of the studied machine, which requires a particular material behavior. Therefore, a most appropriate choice for the material can be done. On the other hand, with the knowledge of the detailed material's property, a tailor-made material can be defined. The knowledge of other magnetic property deterioration due to induced residual stress occurring during the manufacturing as well as due to applied mechanical stresses during the operation of the electrical machine is indispensable for contemporary machine design [7].

Particularly, the cut-edge effect in electrical steel laminations has to be considered, because the local magnetic property deterioration due to induced mechanical stress is significant [8]–[10]. Cutting induces plastic deformation and residual stress in the laminations. The extent of degradation substantially depends on the process characteristics, i.e., the cutting procedure and cutting parameters in combination with material properties, such as mechanical strength and grain size [10]. At this point, cut-edge effects are sparsely considered in

electrical machine simulations. Different models have been published, with the common aim to describe the varying local magnetization and loss behavior. By replacing effortful sliced models, the continuous model (CM) is independent of the discretization and converges in the case of coarse meshes to the sliced model [11]. Measured single-sheet specimens are used to identify different model parameters. The vital advantage of the proposed CM is that properties depend only on the distance to the cut edge. For improved estimation of penetration depth and mechanical stress distribution, the novel experimental procedures are utilized [12] and mechanical simulations are evaluated [10] to further advance the cut-edge model.

In permanent-magnet synchronous and flux-switching machines, in addition to the soft-magnetic material, the permanent magnets are central to the electromagnetic energy conversion process. In order to design the magnetic circuit and a magnetizing circuit for post-assembly magnetization as well as to analyze the resistance to being demagnetized during the simulation of electrical machines, it is indispensable to describe the magnetization behavior of the permanent magnets accurately. However, due to the complex interplay of the non-linear and hysteretic magnetization behavior and the magnetic anisotropy, it is a complex problem. Commonly, simplified models are used, which are based on empirical and phenomenological approaches. These describe the major loop of only the permanent magnets. However, the magnetization state of the permanent magnet depends on the magnetic and thermic history.

This paper will give an overview of the current modeling approaches applied at IEM for soft- and hard-magnetic materials in the simulation of rotating electrical machines. For this, the inhouse solver pyMOOSE is utilized. Efficient parametric models with low additional computational effort are perfectly suited for the finite-element (FE) analysis. Starting from these advanced models of soft- and hard-magnetic materials, a methodology for selecting the optimal steel grade during the design stage of electrical machines in due consideration of the application-specific requirements on torque–speed operating points can be enabled in the future. This can allow one to study the effect of different electrical steel grades on the operational characteristics along the torque–speed map.

II. Modeling of Soft- and Hard-Magnetic Materials

A. Iron-Loss Modeling

For the estimation of iron losses in soft-magnetic materials over a broad frequency and magnetic flux range, different models have been proposed. These models can be prescribed along with an axis between empirical and physical approaches. The following Steinmetz equation is a sole fit on measurement data and limited to sinusoidal waveforms and, therefore, the most empirical equation used for iron-loss modeling. It is based on an equation proposed by Steinmetz [13], which at this point was formulated without the frequency dependence of today's version

$$P_{\text{Steinmetz}} = k f^{\alpha} \hat{B}^{\beta} \tag{1}$$

where $\hat{B}$ is the peak value of the flux density, f is the frequency, and k, α and β are fitting parameters. This equation was evolved by Jordan [14] to include the impact of eddy-current losses and by Pry and Bean [15] to include the effect of excess losses in term of an additional loss factor on eddy current loss. With this expression, the role of domain walls was considered in loss calculation. Bertotti [16] included the excess loss as an additional term and identified the $\hat{B}$ and f dependence in his basic formulation as follows:

$$P_{\text{Bertotti}} = C_{\text{hyst}} \hat{B}^2 f + C_{\text{cl}} \hat{B}^2 f^2 + C_{\text{exc}} (\hat{B} f)^{1.5} \tag{2}$$

where C_{hyst}, C_{cl}, and C_{exc} are factors for the hysteresis, classical eddy current, and excess losses. Based on the statistical loss theory, the physical interpretation of the terms enables the correlation between the different loss terms and relevant material parameters, e.g., grain size, sheet thickness, domain wall configuration, and mechanical stress [17].

Although the Bertotti model is often used for iron-loss modeling and has the benefit of a comprehensive physical explanation, it has a weakness in the estimation of loss at high frequencies and inductions. The IEM Formula as introduced in [5] adds an additional term to the loss equation to account for non-linear material behavior. It is shown in [5] and [18] that the classical Bertotti model [16] underestimates losses at high magnetic flux densities and high frequencies. This is linked to the neglect of saturation. The IEM-Formula shows a significant improvement in loss determination at high magnetic flux densities and high frequencies, due to a fourth loss term with a higher order dependence that is added to the equation. This results in the following mathematical formulation:

$$P_{\text{IEM}} = a_1 \hat{B}^{\alpha + \hat{B}\beta} f + a_2 \hat{B}^2 f^2 (1 + a_3 \hat{B}^{a_4}) + a_5 (\hat{B} f)^{1.5}. \tag{3}$$

Formula (3) describes the total iron loss as a contribution of hysteresis losses, classical Foucault eddy current losses, excess losses, and a fourth term called saturation or non-linear losses. In this equation, a_i and α, β are the fit material parameters. The identification process is based on the statistical loss theory [19]. The hysteresis parameters a_1 and α can be determined from point-by-point dc-measurements according to the following equation:

$$E_{\text{dc}} = a_1 \hat{B}^{\alpha + \hat{B}\beta}. \tag{4}$$

For calculation of a_2, the sheet thickness d, specific density ρ and specific electrical resistivity ρ_{el} are taken into account, according to the classical Foucault eddy-current losses in the following equation:

$$a_2 = \frac{\pi^2 d^2}{6 \rho \rho_e}. \tag{5}$$

The excess loss parameter a_5 can either be identified by measurements at relatively low magnetic flux densities and frequencies between 5 and 10 Hz or calculated solely from material-dependent properties. For the first approach, the excess loss term is separated from measurements below 10 Hz by subtraction of the preliminary described hysteresis (4) and classical Foucault eddy current losses (5). At these frequencies, saturation losses are neglected. The second approach is based on the theory of magnetic objects,

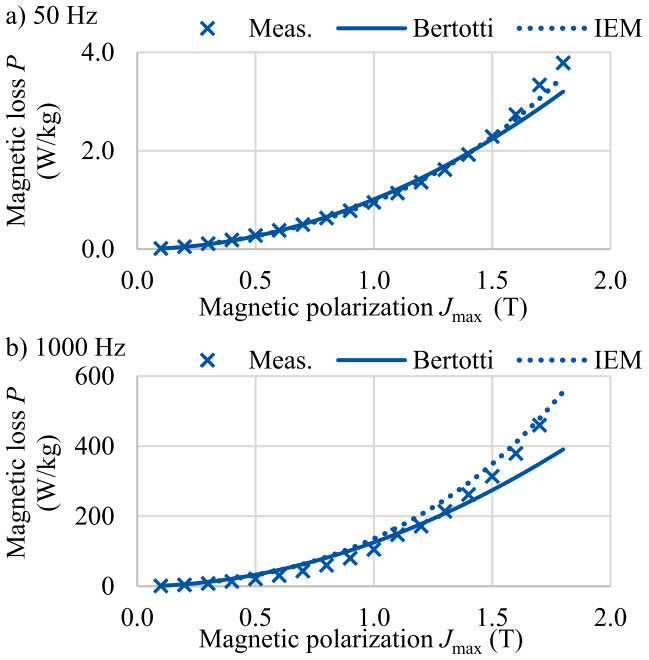

Fig. 1. Comparison of the IEM formula with the Bertotti model and measurement results for M270-50A at (a) 50 and (b) 1000 Hz.

increased in number by eddy current magnetic fields due to an increase of magnetizing frequency [16]. At last, the parameters a_3 and a_4 are parametrized from the nonlinear material behavior at high frequencies and magnetic flux densities. Thus, the iron-loss terms of the IEM (3) are identified.

The proposed semi-physical loss model is still an approximation to actual material behavior. Especially (5) has shown to be inaccurate [20]. The use of numerical models as presented in [21] can increase the accuracy. As discussed in the Introduction, hysteresis models could improve the accuracy as well. However, during the design of electrical machines, the consideration of the entire speed–torque characteristic is important and, therefore, material models need to have low additional computational effort. The enhancement of either computational effort or accuracy of different models is a strong focus of various studies. Zirka *et al.* [20] noted the simplified loss prediction routines as presented here are still an acceptable approximation for loss modeling.

In Fig. 1(a), the comparison of the IEM model (3) to the Bertotti model (2) is depicted at two frequencies for a conventional M270-50A. Especially at high frequencies, the relative error between measured and estimated iron loss is distinctly smaller compared with the Bertotti model, i.e., +4% to −30% at 1.7 T and 1000 Hz. This shows that the approximation of losses up to 1000 Hz is good for this material. The parameter identification is obtained by the standardized Epstein/single-sheet-tester (SST) measurements on an MPG system by Brockhaus measurement systems at quasi-static (dc) excitation and frequencies up to 5000 Hz. The samples for material characterization are supposed to be produced carefully, with non-degrading procedures such as spark erosion or waterjet cutting in order to maintain the materials' properties. At-large SST geometries, the cutting effect has a negligible effect. In the case of a 120 mm × 120 mm SST, this has been shown in [10] and [22]. For smaller geometries, in material characterization as well as actual electric machines, however, cutting has a significant effect on the magnetic properties of the steel. As a result, the loss parameters from standardized testing do not represent the behavior to be expected in cut and packaged motor core laminations but in the virgin material.

Krings and Soulard [23] present an overview of influencing factors with a focus on manufacturing, on the different loss terms from classical loss separation. Although relations can be concluded the effects of manufacturing are mainly local and need to be included and modeled accordingly. This highlights the need to improve the modeling of the impact of processing on iron losses in FE machine simulation. Thereby, a higher accuracy of models can be targeted.

B. Influence of Processing

As mentioned, the magnetic properties of electrical steel are highly sensitive to mechanical stress [24], [25]. Due to the magnetoelastic and magnetoelasticplastic coupling, residual stress as a result of cutting can alter the magnetic properties significantly. Each processing steep from cutting to stacking and fixing induces residual stress in the electrical steel lamination [26]. An extension of the IEM iron-loss model was proposed from [6] and incorporates the impact of mechanical stress σ on the parameters a_i and α, β as follows:

$$P_{\mathrm{IEM}}(\sigma) = a_1(\sigma)\hat{B}^{\alpha(\sigma)+\hat{B}\beta(\sigma)} f + a_2 \hat{B}^2 f^2 (1 + a_3(\sigma)\hat{B}^{a_4(\sigma)}) + a_5(\sigma)(\hat{B} f)^{1.5}. \quad (6)$$

The cutting process specifically has been subject to various studies and has been characterized in great detail. In general, cutting is highly detrimental to the electromagnetic properties of electrical steel, i.e., it increases losses and decreases permeability and magnetizability. Different cutting techniques influence the properties to a different extent [8], [27], [28]. The reason is the physical impact on the material, primarily the mechanism of material separation, e.g., thermal, mechanical or abrasive material separation from cutting techniques as shear, laser or abrasive waterjet cutting, as well as the cutting parameters themselves [10].

Additional complexity comes from the fact that general measures to limit losses in electrical steel are disadvantageous to what generally is deemed beneficial to the cutting process. Increasing silicon content increases the resistivity, which, in addition to small sheet thicknesses, reduces classical eddy currents [17], [23], [29]. Generally, grain sizes for electrical steel are relatively coarse, due to the resulting low hysteresis loss with grains of an average diameter of about 70 to 150 μm for conventional grades. A minimum of total loss identified by [30] is of about 100 μm, however, depending on the frequency, due to the loss component distribution. These measures are unfavorable for the cutting because silicon content degrades cold formability, and therefore obstructs the cutting process. Meager cold formability, thin sheets, and large grains result in undefined crack mechanisms, i.e., inter- and trans-crystalline cracking. However, it is not yet evinced,

if undefined crack mechanisms and unfavorable cutting behavior are actually detrimental to magnetic properties.

With improved modeling, the tradeoff between sheet, thickness, silicon content, and sensitivity to cutting can be evaluated from the final application and design choices can be based on FE machine simulations. Therefore, the effect of cutting needs to be included in the FE modeling.

Consistently, a model has been developed at the IEM to describe the continuous local material properties, which can be used in FE simulation [31]. Depending on geometrical, material and processing parameters along with the magnetic field strength, the iron losses resulting from different cutting techniques can differ by a factor of two or higher, due to increasing static and dynamic hysteresis losses [7], [32]–[34]. Determining the local magnetic properties of soft-magnetic materials used, for example, in electrical machinery, therefore, is an essential part to consider in the design and FE simulations. To cope with continuous, locally changing material properties different models have been published describing local permeability distributions [35]–[37] or the resulting iron losses [38] and are compared in [11].

Standardized measurement frames use specimen sizes of 30 and 120 mm width for Epstein and SST, respectively. As the manufacturing influence on the magnetic properties of the lamination gets more pronounced at smaller strip width or a higher ratio of total cutting length to the volume, standardized specimen widths underestimate the resulting specific iron losses in rotating electrical machines. To consider the manufacturing influences on the resulting magnetization and iron-loss behavior, material samples of different sizes according to the application's geometry must be characterized. In order to identify the model parameter of the developed local material model, single-sheet specimens are cut according to the manufacturing process used for the actual application. Starting with a square of 120 mm × 120 mm, the samples are cut consecutively to different strip widths b, as depicted in Fig. 2(a), while keeping the total cross section constant. The specimens are used for the parametrization of both the continuous local material model and the iron losses depicted in Fig. 2(b). The model written in the following equation is presented in [39] and describes the local permeability μ_r as a function of the undamaged permeability $\mu_{r,\mathrm{und}}$, the distance to the cut edge or the local deterioration profile $\eta(x)$, and the maximum permeability drop at the cut surface $\Delta\mu_{\mathrm{cut}}$:

$$\mu_r(x) = \mu_{r,\mathrm{und}}(H) - \eta(x) \cdot \Delta\mu_{\mathrm{cut}}(H). \tag{7}$$

The shape of the local deterioration profile depends on the technique used for the cutting process in combination with the material. Especially in the case of mechanical cutting such as blanking a parabolic distribution can be assumed [40], [41]. Therefore, the model can represent the resulting local magnetic properties according to the specific cutting technique.

The local deterioration profile is defined in the following equation within the influence depth δ, with a being the slope of the local deterioration function. The local deterioration is one key parameter of the model and can be identified using

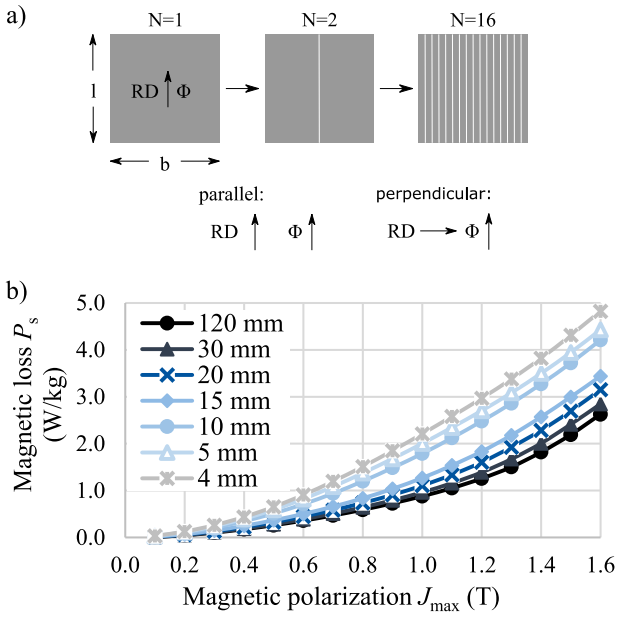

Fig. 2. (a) Sample preparation for single-sheet measurements of different strip widths b to consider cut-edge effects due to manufacturing in iron-loss measurements and (b) specific iron losses at 50 Hz of different specimen widths.

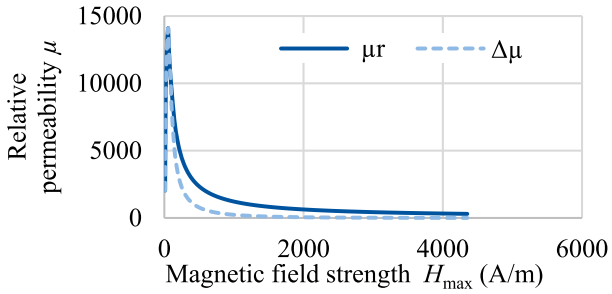

Fig. 3. Measured undamaged relative permeability μ_r and resulting permeability drop at the cut-edge $\Delta\mu_{\mathrm{cut}}$ at 50 Hz.

the magnetic characterizations described before

$$\eta(x) = \begin{cases} 1 - \dfrac{x}{\delta} - a\dfrac{x}{\delta}\left(1 - \dfrac{x}{\delta}\right) & \text{for } 0 < x \le \delta \\ 0 & \text{for } x > \delta. \end{cases} \tag{8}$$

The maximum permeability drop at the cut edge defined in the following equation has to be identified such that $\Delta\mu_{\mathrm{cut}}$ is independent on the strip width:

$$\Delta\mu_{\mathrm{cut}}(H) = \frac{\mu_{r,\mathrm{und}}(H) - \mu_r(H,b)}{F(b)} = \text{const } \forall b. \tag{9}$$

Hence, the function value $F(b)$ describes the integral value of the local deterioration $\eta(x)$. The resulting permeability drop at the cut edge $\Delta\mu_{\mathrm{cut}}$ is presented in Fig. 3 along with the undamaged permeability. The model parameter of the local deterioration profile results in $a = 1$ and $\delta = 6.5$ mm.

In order to use the continuous material model in FE-simulations, an algorithm assigning each element a corresponding minimal distance to the cut surface is implemented. The distance of the element to the cutting edge is stored as an additional property of the mesh element.

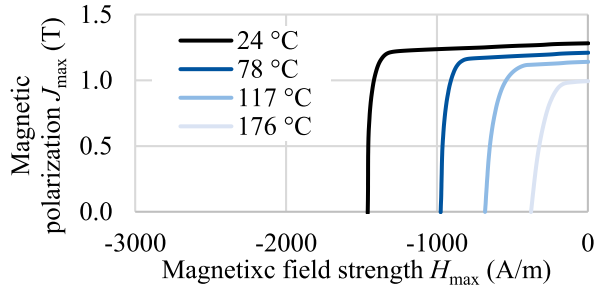

Fig. 4. Temperature dependence of B_r and H_{cJ} for VACODYM764AP.

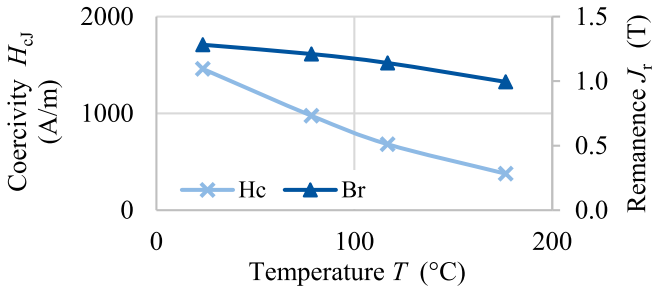

Fig. 5. Temperature dependence of B_r and H_{cJ} for VACODYM764AP.

C. Hard-Magnetic Material Modeling

For permanent magnets, in contrast to the soft magnetics, the focus is to ensure the working point and load line at a given temperature within the reversible region of demagnetization. The resulting losses are only relevant with respect to possible temperature caused irreversible demagnetization and are mainly based on electrical conductivity and not on magnetic hysteresis. Especially the modeling of 3-D eddy currents in 2-D electrical machine simulation with permanent magnets is a challenging problem [42].

In [43], a nonlinear temperature-dependent model for permanent magnet demagnetization is proposed. The temperature-dependent equation for the magnetic polarization is as follows:

$$J(H,T) = P(T)\left(b_0 \tanh\left(\frac{H+Q(T)H_{cJ}(T_0)}{Q(T)h_0}\right) + b_1 \tanh\left(\frac{H+Q(T)H_{cJ}(T_0)}{Q(T)h_1}\right)\right). \quad (10)$$

The coefficients $b_{0,1}$ und $h_{0,1}$ are identified by a nonlinear curve fitting of the major demagnetization line at temperature T_0. The temperature-dependent terms of (10) for the remanence $P(T)$ and coercivity $Q(T)$ are approximated with a quadratic function with two temperature coefficients each

$$\begin{matrix} B_r(T) \\ H_{cJ}(T) \end{matrix} = \begin{matrix} B_r(T_0) \\ H_{cJ}(T_0) \end{matrix}\left(1 + \begin{matrix} \alpha_1 \\ \beta_1 \end{matrix}(T-T_0) + \begin{matrix} \alpha_2 \\ \beta_2 \end{matrix}(T-T_0)^2\right) = \begin{matrix} B_r(T_0)P(T) \\ H_{cJ}(T_0)Q(T) \end{matrix}. \quad (11)$$

The magnetic polarization of a rare-earth NdFeB permanent magnet over the magnetic field is shown for different temperatures in Fig. 4. The measurements are performed with a pulsed-field magnetometer based on open magnetic circuit described in the pre-standard IEC-V 42331. The corresponding of B_r and H_{cJ} over temperature is plotted in Fig. 5. The model parameters are identified for the samples listed in Table I and summed up in Table II. For the same materials, a pragmatic methodology to replicate the hysteresis is presented, which uses the first-order return curves and the magnetization behavior starting from the virgin state for model parameter identification without concerning temperature dependence [44]. A temperature-dependent vector hysteresis model for permanent magnets is proposed in [45].

All models contain a nonlinearity which needs to be represented in the FE simulation with either the fixed point: $\nabla \times (\nu_{FP}\nabla \times A^k) = J + \nabla \times ((\nu_{FP} - \nu^{k-1})\nabla \times A^{k-1})$ or a (differential) Newton approach: $\nabla \times (\nu_d(B^{k-1})\nabla \times A^k = J - \nabla \times H^{k-1}$.

TABLE I
MEASURED RARE-EARTH PERMANENT-MAGNET SAMPLES

Name	Vacodym 764	Vacodym 890	Vacomax 170	Vacomax 262
Pressing direction	AP	AP	HR	HR
IEC60404-8-1	305/135.5	210/263	170/120	143/175
B_r in T	1.3	1.11	1.01	1.19
H_{cj} in kA/m	1355	2625	1195	1750
Mat. T.	NdFeB	NdFeB	$SmCo_5$	Sm_2Co_{17}
Mag. T.	nucleation	nucleation	nucleation	Pinnig
Shape	cylinder	cylinder	cylinder	Block
Size mm	15x5.5	10x10	10x10	24x17x5
Demag. coeff.	0.55	0.32	0.32	0.65

TABLE II
THERMAL DEMAGNETIZATION MODEL PARAMETER IDENTIFICATION

Name		Vacodym 764	Vacodym 890	Vacomax 170	Vacomax 262
T_0	in °C	23.42	23.25	23.41	24.42
$B_r(T_0)$	in T	1.282	1.118	0.9177	1.179
$b_0(T_0)$	in T	0.32	0.67	0.07	1.06
$b_1(T_0)$	in T	0.96	0.44	0.84	0.12
α_1	in 1/K	-7.55e-4	-1.12e-3	-1.19e-4	-1.73e-4
α_2	in $1/K^2$	-4.64e-6	-1.72e-6	-3.99e-6	-3.45e-6
$H_{cJ}(T_0)$	in kA/m	1459	2833	1063	2283
$h_0(T_0)$	in kA/m	1.294e-3	5.572	6.407e-3	202.1
$h_1(T_0)$	in kA/m	107.1	235.7	690.2	1865
β_1	in 1/K	-6.87e-3	-4.69e-3	-2.49e-3	-2.64e-3
β_2	in $1/K^2$	1.316e-5	4.705e-6	2.262e-6	5.593e-7

III. APPLICATION OF MODELS TO A CASE EXAMPLE AND DISCUSSION

In the case study, previously discussed methodologies are used to compare two different electric vehicle range simulations, i.e., with and without consideration of cutting effects using guillotine cutting.

A. Identification of Loss Parameters

For the investigation of the influence of different cutting techniques on the range of an electric car, sheets with different strip widths w_{st} are cut and magnetically measured on an SST as presented in [46]. In this paper, the material M270-35A is

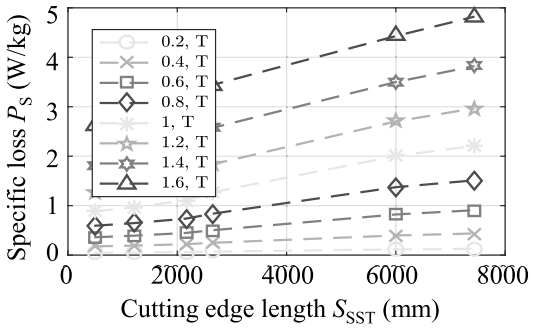

Fig. 6. Specific losses of M270-35A measured in parallel to the rolling direction.

TABLE III
TECHNICAL DATA OF THE STUDIED PMSM

Specification	Value
Number of pole pairs p	6
Peak torque T_{peak}	190 Nm
Peak Power P_{peak}	85 kW
Maximum rotational speed n_{max}	10000 rpm

cut with w_{st} from 4 to 120 mm in a total of six steps using guillotine shears. The length of all specimens l_{tot} is 120 mm. The measured magnetization properties are used for the local magnetization model. The length of the cut-edge S_{SST} of each probe can be calculated with

$$S_{\text{SST}} = 2w_{\text{tot}} + 2\frac{w_{\text{tot}}}{w_{\text{st}}}l_{\text{tot}}. \tag{12}$$

The specific losses P_s of the sheet in dependence of the polarization J and S_{SST} are shown in Fig. 6. The losses show a linear dependence to the length of the cut-edge S_{SST}.

B. FEM Simulation Model

For studying the influence of cutting techniques on vehicle range, a fully electric drivetrain with a permanent-magnet synchronous motor (PMSM) is chosen. The data sheet of the motor is shown in Table III.

For the determination of loss parameters, the cut length of the stator S_{Stat} and the rotor S_{Rot} are determined separately. The equivalent cut-edge length of the stator S'_{Stat} and the rotor S'_{Rot} needs to be calculated using the following formula:

$$S'_{\text{Stat}} = S_{\text{Stat}}\frac{w_{\text{tot}}l_{\text{tot}}}{A_{\text{Stat}}} \tag{13}$$

where A_{Stat} is the area of the stator lamination and the rotor, respectively. First, the measured data (see Fig. 6) are interpolated by the equivalent cut-edge length of the stator S'_{Stat} and the rotor S'_{Rot} to get equivalent losses. For the identification of the loss parameters, the methodology introduced in [46] is used. Both the equivalent cut-edge length of the stator and the rotor are greater than 4000 mm. Due to this lamination design, significant impact on the losses of the electric machine in the drive cycle is expected.

TABLE IV
TECHNICAL DATA OF THE VEHICLE MODEL

Specification	Value
Friction coefficient f_{fric}	0.01
vehicle mass m_{veh}	1500 kg
additional mass m_{add}	500 kg
Slope angle φ	0°
Air density ρ_{Air}	1.204 kg/m^3
Air friction coefficient c_W	0.3
Vehicle cross section A	2.5
Acceleration coefficient e_i	1.044

C. Vehicle Range Model

The calculated efficiency plots in the torque–speed map can be used for calculating the vehicle range in various drive cycles. This paper is a substantial electric machine design tool to ensure proper focus in the design process. The simulation methodology for the utilization of different lamination materials is shown in [1]. In order to estimate the realistic impact of the electric machine design on the driving range, a simple vehicle model for the longitudinal dynamics of a fully electric car is used. The actual power needed in the drive cycle $P_{\text{Cycle}}(t)$ can be calculated with the following equation [47]:

$$P_{\text{Cycle}}(t) = (F_{\text{Roll}}(t) + F_{\text{Air}}(t) + F_{\text{Slope}}(t) + F_{\text{Acc}}(t))v(t). \tag{14}$$

The forces in the tread of the tire for the rolling friction F_{roll}, the air friction F_{Air}, the slope F_{slope}, and the acceleration F_{Acc} are determined based on the formula introduced in [4] using the following equations:

$$F_{\text{Roll}} = f_{\text{fric}} \cdot (m_{\text{veh}} + m_{\text{add}})\cos(\varphi) \tag{15}$$

$$F_{\text{Air}}(t) = \frac{1}{2}\rho_{\text{Air}} c_W A v(t)^2 \tag{16}$$

$$F_{\text{Slope}} = (m_{\text{veh}} + m_{\text{add}})\sin(\varphi) \tag{17}$$

$$F_{\text{Acc}} = (m_{\text{veh}}e_i + m_{\text{add}})\frac{dv(t)}{dt} \tag{18}$$

where $v(t)$ is the vehicle velocity. For the vehicle model symbols, typical values for a small city car are selected as shown in Table IV.

For calculation of the necessary battery power of the electric car, the following formula is used:

$$P_{\text{Bat}}(t) = \eta_{\text{In,Bat}}^{\varepsilon}\eta_{\text{Mot}^{\varepsilon}}(t)\eta_{\text{GB,Diff}}^{\varepsilon}P_{\text{Cycle}}(t) \tag{19}$$

where $\eta_{\text{In,Bat}}$ is the combined efficiency of inverter and battery and $\eta_{\text{GB,Diff}}$ is the combined efficiency of the gearbox and the differential. To reduce model complexity, $\eta_{\text{In,Bat}}$ as well as $\eta_{\text{GB,Diff}}$ are assumed to be constant with $\eta_{\text{In,Bat}} = 95\%$ and $\eta_{\text{GB,Diff}} = 97\%$. The coefficient ε depends on the operation mode, i.e., $\varepsilon = 1$ for driving mode and $\varepsilon = -1$ for recuperation mode. Other influences are neglected. In a more detailed study of the entire powertrain, detailed simulation of the loss parameters can easily be added. In this paper, these impacts are not considered in detail, as electric machine design parameters are in focus of the investigation. The efficiency of the electric

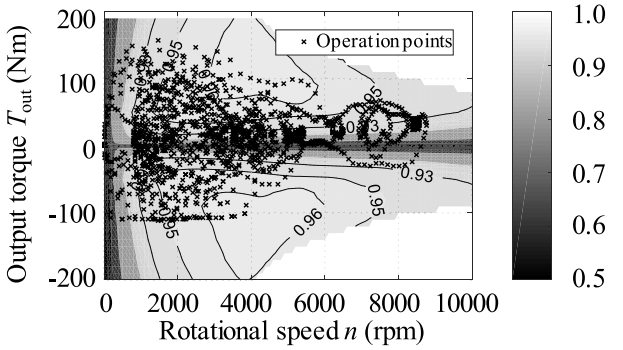

Fig. 7. Efficiency of the electric motor η_{Mot} and operation points of the simulation without consideration of cutting effect.

TABLE V
LOSS POWER IN WLTC CLASS 3

Loss Component	Without cutting effect	With cutting effect guillotine shear
Battery and inverter	579.1 W	585.1 W
Iron loss rotor	106.4 W	143.7 W
Iron loss stator	360.6 W	496.9 W
Copper loss	209.2 W	216.1 W
Gearbox and differential	323.9 W	323.9 W
Rolling friction losses	2535.6 W	2535.6 W
Air friction losses	2991.1 W	2991.1 W
Total battery power $P_{Bat,avg}$	7106.0 W	7292.4 W
Total vehicle Range r_{tot}	163.6 km	159.5 km

motor $\eta_{\text{Mot}}(t)$ is determined based on the efficiency plots generated in the FE simulation. Different driving cycles can be used for the investigation as shown in [47]. In this paper, the worldwide harmonized light vehicles test procedure (WLTP) Class 3 is used. The cycle has a total length of $r_{\text{Cycle}} = 23.3$ km and a duration of $t_{\text{Cycle}} = 1800$ s. The total usable battery energy is assumed to be $E_{\text{Bat}} = 25$ kWh. The range of the car is calculated based on the following formulas:

$$P_{\text{Bat,avg}} = \frac{1}{t_{\text{Cycle}}} \int_{0s}^{t_{\text{Cycle}}} P_{\text{Bat}}(t)dt \tag{20}$$

$$r_{\text{tot}} = r_{\text{Cycle}} \frac{E_{\text{Bat}}}{P_{\text{Bat,avg}} t_{\text{Cycle}}} \tag{21}$$

where $P_{\text{Bat,avg}}$ is the total average battery power used in the cycle.

D. Results

The efficiency plot of the electric motor η_{Mot} as a result of the FE method (FEM) simulation in dependence of the electric motor output torque T_{out} and the rotational speed n of the machine without consideration of the cutting effect are shown in Fig. 7. The needed combination of torque and speed for each operation point in the driving cycle can be calculated based on the defined WLTP Class 3 cycle, the ratio of the gearbox and differential, and the vehicle resistances (15)–(18) as shown in [47]. The distribution of operation points in a discretization of 1 s is shown in Fig. 7. The detailed results of the driving range simulation are shown in Table V.

The motor is assumed to recuperate all braking energy in the driving cycle. Thus, acceleration losses cannot be found in the final loss distribution. Under consideration of cutting effects, the rotor iron losses increase around 35.1%, stator iron losses around 37.8%, and copper losses around 3.2% in comparison to the simulation without consideration of the cutting effect. This sums up in a total decrease of the vehicle range r_{tot} of 2.6% in case cutting effect using guillotine shear is considered in the simulation. The significant influence of the cutting effect on vehicle driving range has several reasons. The used geometry has a significant cut-edge length as discussed previously. This means that the geometrical dimensions of the machine geometry deviate from the SST specimen sizes used in standardized material characterizations. The studied guillotine shear is not optimized in regards to residual stress in the material. The machine is designed with high polarization frequencies causing high iron losses and high impact on overall machine characteristics. The shown methodology was validated on machine measurements in [46].

IV. CONCLUSION

In this paper, advanced models of soft- and hard-magnetic materials that are applied at the IEM are presented. Next to the main target to better understand the material's behavior, the model enhancement results in a better accuracy for efficient parametric models with low additional computational effort, which are well suited for the FE analysis for the simulation of rotating electrical machines.

The consideration of phenomenological effects in machine simulations is indispensable for improved machine modeling. For the soft-magnetic material, the results of the simulations with and without cutting effect show a significant iron loss increase. When cutting effects are taken into account, losses increases >30% for the rotor and stator, in case of the generally very detrimental guillotine cutting in combination with a geometry with a high overall cutting length. The exact calculation of the resulting losses is essential for a further thermal analysis of the machine geometry. For the hard-magnetic materials, in particular, the magnets must not be irreversibly demagnetized even under thermal load in the field weakening region. The interrelation between cutting, geometry iron losses can only be simulated with these advanced models and enable respective considerations, already at the design stage of electrical machines. A framework, comprising the cut-edge model and improved stress-dependent iron-loss modeling further allows the incorporation of other processing influences on the magnetic properties of the material.

Application-specific requirements of torque–speed operating points can be accounted for material selection with regard to the processing. This can enhance the study of the effect of different electrical steel grades on the operational characteristics of electrical machines.

ACKNOWLEDGMENT

This work was supported by Deutsche Forschungsgemeinschaft, German Research Foundation through the Research Group Project "FOR 1897—Low-Loss Electrical Steel for Energy-Efficient Electrical Drives" under Grant 255713208.

REFERENCES

[1] A. Ruf, S. Steentjes, G. von Pfingsten, T. Grosse, and K. Hameyer, "Requirements on soft magnetic materials for electric traction motors," in *Proc. 7th Int. Conf. Magn. Metall. (WMM)*, 2016, pp. 111–128.

[2] M. Filippini, P. Alotto, G. Glehn, and K. Hameyer, "Magnetic transmission gear finite element simulation with iron pole hysteresis," *Open Phys.*, vol. 16, no. 1, pp. 105–110, 2018.

[3] E. Cardelli, "Advances in magnetic hysteresis modeling," in *Handbook of Magnetic Materials*, vol. 24, K. H. J. Buschow, Ed. Amsterdam, The Netherlands: Elsevier, 2015, ch. 4, pp. 323–409.

[4] E. Cardelli *et al.*, "A challenging hysteresis operator for the simulation of goss-textured magnetic materials," *J. Magn. Magn. Mater.*, vol. 432, pp. 14–23, Jun. 2017.

[5] D. Eggers, S. Steentjes, and K. Hameyer, "Advanced iron-loss estimation for nonlinear material behavior," *IEEE Trans. Magn.*, vol. 48, no. 11, pp. 3021–3024, Nov. 2012.

[6] J. Karthaus, S. Steentjes, N. Leuning, and K. Hameyer, "Effect of mechanical stress on different iron loss components up to high frequencies and magnetic flux densities," *COMPEL, Int. J. Comput. Math. Elect. Electron. Eng.*, vol. 36, no. 3, pp. 580–592, 2017.

[7] S. Steentjes, G. von Pfingsten, and K. Hameyer, "An application-oriented approach for consideration of material degradation effects due to cutting on iron losses and magnetizability," *IEEE Trans. Magn.*, vol. 50, no. 11, Nov. 2014, Art. no. 7027804.

[8] M. Emura, F. J. G. Landgraf, W. Ross, and J. R. Barreta, "The influence of cutting technique on the magnetic properties of electrical steels," *J. Magn. Magn. Mater.*, vols. 254–255, pp. 358–360, Jan. 2003.

[9] N. Leuning, S. Steentjes, K. Hameyer, M. Schulte, and W. Bleck, "Effect of material processing and imposed mechanical stress on the magnetic, mechanical, and microstructural properties of high-silicon electrical steel," *Steel Res. Int.*, vol. 87, no. 12, pp. 1638–1647, 2016.

[10] H. A. Weiss *et al.*, "Influence of shear cutting parameters on the electromagnetic properties of non-oriented electrical steel sheets," *J. Magn. Magn. Mater.*, vol. 421, pp. 250–259, Jan. 2017.

[11] S. Elfgen, S. Steentjes, S. Böhmer, D. Franck, and K. Hameyer, "Continuous local material model for cut edge effects in soft magnetic materials," *IEEE Trans. Magn.*, vol. 52, no. 5, May 2016, Art. no. 2001304.

[12] H. A. Weiss *et al.*, "Targeted local stress imprint in electrical steel as means of improving the energy efficiency," in *Proc. 4th Int. Conf. X-Ray Neutron Phase Imag. With Gratings (XNPIG)*, Zürich, Switzerland, 2017.

[13] C. P. Steinmetz, "On the law of hysteresis," *Proc. IEEE*, vol. 72, no. 2, pp. 197–221, Feb. 1984.

[14] H. Jordan, *Die Ferromagnetischen Konstanten für schwache Wechselfelder*. ENT 1, 1924.

[15] R. H. Pry and C. P. Bean, "Calculation of the energy loss in magnetic sheet materials using a domain model," *J. Appl. Phys.*, vol. 29, pp. 532–533, Mar. 1958.

[16] G. Bertotti, *Hysteresis in Magnetism: For Physicists, Materials Scientists, and Engineers*. New York, NY, USA: Academic, 1998.

[17] G. Bertotti, "General properties of power losses in soft ferromagnetic materials," *IEEE Trans. Magn.*, vol. MAG-24, no. 1, pp. 621–630, Jan. 1988.

[18] S. Jacobs, F. Henrotte, M. H. Gracia, K. Hameyer, P. Goes, and D. Hectors, "Magnetic material optimization for hybrid vehicle PMSM drives," presented at the Inductica Conf., Chicago, IL, USA, 2009.

[19] S. Steentjes, M. Leßmann, and K. Hameyer, "Semi-physical parameter identification for an iron-loss formula allowing loss-separation," *J. Appl. Phys.*, vol. 113, no. 17, p. 17A319, 2013.

[20] S. E. Zirka, Y. I. Moroz, P. Marketos, and A. J. Moses, "Loss separation in nonoriented electrical steels," *IEEE Trans. Magn.*, vol. 46, no. 2, pp. 286–289, Sep. 2010.

[21] S. E. Zirka, Y. I. Moroz, P. Marketos, and A. J. Moses, "Viscosity-based magnetodynamic model of soft magnetic materials," *IEEE Trans. Magn.*, vol. 42, no. 9, pp. 2121–2132, Sep. 2006.

[22] H. A. Weiss *et al.*, "Loss reduction due to blanking parameter optimization for different non-grain oriented electrical steel grades," in *Proc. IEEE Int. Electr. Mach. Drives Conf. (IEMDC)*, May 2017, pp. 1–7.

[23] A. Krings and J. Soulard, "Overview and comparison of iron loss models for electrical machines," in *Proc. Ecol. Vehicles Renew. Energies*, Monaco, U.K., Mar. 2010.

[24] R. M. Bozorth, *Ferromagnetism*. New York, NY, USA: Van Nostrand, 1951.

[25] V. E. Iordache, F. Ossart, and E. Hug, "Magnetic characterisation of elastically and plastically tensile strained non-oriented Fe–3.2%Si steel," *J. Magn. Magn. Mater.*, vols. 254–255, pp. 57–59, Jan. 2003.

[26] G. E. Totten, T. Inoue, and M. Howes, *Handbook of Residual Stress and Deformation of Steel*. New York, NY, USA: ASM, 2002.

[27] E. G. Araujo, J. Schneider, K. Verbeken, G. Pasquarella, and Y. Houbaert, "Dimensional effects on magnetic properties of Fe–Si steels due to laser and mechanical cutting," *IEEE Trans. Magn.*, vol. 46, no. 2, pp. 213–216, Feb. 2010.

[28] Y. Kurosaki, H. Mogi, H. Fujii, T. Kubota, and M. Shiozaki, "Importance of punching and workability in non-oriented electrical steel sheets," *J. Magn. Magn. Mater.*, vol. 320, no. 20, pp. 2474–2480, 2008.

[29] M. Littmann, "Iron and silicon-iron alloys," *IEEE Trans. Magn.*, vol. MAG-7, no. 1, pp. 48–60, Mar. 1971.

[30] M. Bölling, K. Espenhahn, K. Guhnter, M. Hastenrath, and R. Huneus, "Trends und Ziele in der Entwicklung hochwertiger Elektrobleche," *Stahl Eisen*, vol. 245, no. 107, pp. 1119–1124, 1987.

[31] S. Elfgen, S. Steentjes, S. Böhmer, D. Franck, and K. Hameyer, "Influences of material degradation due to laser cutting on the operating behavior of PMSM using a continuous local material model," *IEEE Trans. Ind. Appl.*, vol. 53, no. 3, pp. 1978–1984, May/Jun. 2017.

[32] A. J. Moses, N. Derebasi, G. Loisos, and A. Schoppa, "Aspects of the cut-edge effect stress on the power loss and flux density distribution in electrical steel sheets," *J. Magn. Magn. Mater.*, vols. 215–216, pp. 690–692, Jun. 2000.

[33] A. Schoppa, J. Schneider, and C.-D. Wuppermann, "Influence of the manufacturing process on the magnetic properties of non-oriented electrical steels," *J. Magn. Magn. Mater.*, vols. 215–216, pp. 74–78, Jun. 2000.

[34] P. Baudouin, M. De Wulf, L. Kestens, and Y. Houbaert, "The effect of the guillotine clearance on the magnetic properties of electrical steels," *J. Magn. Magn. Mater.*, vol. 256, nos. 1–3, pp. 32–40, 2003.

[35] G. Crevecoeur, P. Sergeant, L. Dupré, L. Vandenbossche, and R. van de Walle, "Analysis of the local material degradation near cutting edges of electrical steel sheets," *IEEE Trans. Magn.*, vol. 44, no. 11, pp. 3173–3176, Nov. 2008.

[36] M. Bali, H. De Gersem, and A. Muetze, "Finite-element modeling of magnetic material degradation due to punching," *IEEE Trans. Magn.*, vol. 50, no. 2, pp. 745–748, Feb. 2014.

[37] K. Fujisaki *et al.* "Motor core iron loss analysis evaluating shrink fitting and stamping by finite-element method," *IEEE Trans. Magn.*, vol. 43, no. 5, pp. 1950–1954, May 2007.

[38] B. Hribernik, "Influence of cutting strains on the magnetic anisotropy of fully processed silicon steel," *J. Magn. Magn. Mater.*, vol. 26, nos. 1–3, pp. 72–74, Mar. 1982.

[39] S. Elfgen, S. Böhmer, S. Steentjes, D. Franck, and K. Hameyer, "Continuous model of magnetic material degradation due to cutting effects in the numerical simulation of electro laminations," in *Proc. ETG/GMM-Symp. Innov. Small Drives Micro-Motor Syst.*, Sep. 2015, pp. 1–6.

[40] V. Maurel, F. Ossart, and R. Billardon, "Residual stresses in punched laminations: Phenomenological analysis and influence on the magnetic behavior of electrical steels," *J. Appl. Phys.*, vol. 93, no. 10, pp. 7106–7108, 2003.

[41] F. Ossart, E. Hug, O. Hubert, C. Buvat, and R. Billardon, "Effect of punching on electrical steels: Experimental and numerical coupled analysis," *IEEE Trans. Magn.*, vol. 36, no. 5, pp. 3137–3140, Sep. 2000.

[42] S. Steentjes, S. Boehmer, and K. Hameyer, "Permanent magnet eddy-current losses in 2-D FEM simulations of electrical machines," *IEEE Trans. Magn.*, vol. 51, no. 3, pp. 1–4, Mar. 2015.

[43] P. Zhou, D. Lin, Y. Xiao, N. Lambert, and M. A. Rahman, "Temperature-dependent demagnetization model of permanent magnets for finite element analysis," *IEEE Trans. Magn.*, vol. 48, no. 2, pp. 1031–1034, Feb. 2012.

[44] G. Glehn, S. Steentjes, and K. Hameyer, "Pulsed-field magnetometer measurements and pragmatic hysteresis modeling of rare-earth permanent magnets," *IEEE Trans. Magn.*, vol. 54, no. 3, Mar. 2018, Art. no. 2100404.

[45] A. Bergqvist, D. Lin, and P. Zhou, "Temperature-dependent vector hysteresis model for permanent magnets," *IEEE Trans. Magn.*, vol. 50, no. 2, pp. 345–348, Feb. 2014.

[46] S. Elfgen, A. Ruf, S. Steentjes, and K. Hameyer, "Consideration of the manufacturing influence in standardized material characterizations using machine measurements," in *Proc. IEEE Int. Electr. Mach. Drives Conf. (IEMDC)*, May 2017, pp. 1–6.

[47] L. Eckstein, *Längsdynamik von Kraftfahrzeugen—Verkehrssystem Kraftfahrzeug, Kräfte am Fahrzeug, Antriebstrang, Bremsen, Fahrleistungen und Verbrauch; Vorlesungsumdruck Fahrzeugtechnik I Zitieren*, 4th ed. Aachen, Germany: Forschungsges. Kraftfahrwesen, 2011.